Modulating the Buckling Energy Barrier in Thin-Shell Structures Through Local Imperfections

Azadeh Fathi*, Siamand Lalisani†, Fabien Royer‡
Sibley School of Mechanical and Aerospace Engineering, Cornell University, 124 Hoy Rd, Ithaca, 14853 NY, USA

Thin-shell structures, integral to ultra-lightweight deployable systems, face challenges due to their extreme sensitivity to imperfections, which can significantly influence their buckling stability. We employ a perturbation approach to quantify the effects of local geometric imperfections on the buckling energy barrier. A probing methodology is used to map stability landscapes, quantify energy barriers, and explore the buckling behavior of both perfect and imperfect geometries. Through finite element simulations, this study demonstrates how localized imperfections can either enhance or erode the buckling energy barrier depending on their location, amplitude, and width. Negative dimples significantly lower the resistance to buckling, which often results in an early spontaneous collapse, whereas positive dimples mainly enhance stability up to a specific threshold, after which structural integrity is threatened. Furthermore, we demonstrate that the influence of the width of the imperfection follows three distinct regimes, and that there exists a critical threshold beyond which the minimum load required to initiate buckling under disturbances increases. The findings provide effective strategies to utilize imperfections for modulating the buckling energy barrier, thus enhancing the performance of thin shells.

I. Nomenclature

M_{cr-lin}	=	Linear buckling moment
M_y^0	=	Preloading bending moment
F_p	=	Reaction force at the probe location
D_p	=	Probe displacement
Z_p	=	Probe location
Z_d	=	Dimple location

Presented as Paper 2025-1197 at the AIAA SciTech, Orlando, FL,January 6–10, 2025.

*PhD Student, Sibley School of Mechanical and Aerospace Engineering, Cornell University. AIAA Student Member.
†PhD Student, Sibley School of Mechanical and Aerospace Engineering, Cornell University. AIAA Student Member.
‡Assistant Professor, Sibley School of Mechanical and Aerospace Engineering, Cornell University; fabienr@cornell.edu. AIAA Member (Corresponding Author).

δ = Peak amplitude of the dimple

σ = Gaussian width of the dimple

EB = Energy barrier

α = Angular offset from the middle line

θ = Shell opening angle

R = Shell mid-surface radius

t = Shell thickness

L = Shell length

II. Introduction

The advancement of space technology is closely tied to the development of ultra-lightweight structures, which serve as a foundation for the implementation of larger space systems. These developments hold life-changing potential for Earth's sustainability, particularly through the design of innovative space structures, such as larger space solar power satellites [1, 2]. As the size of these structures increases, so does the generation of clean energy and their contribution to environmental sustainability. Coilable thin-shell structures, with their exceptional properties, have enabled lightweight deployable space structures, which, in turn, facilitate the development of large-scale space systems [3, 4]. To realize larger space structures, further developments in thin shells are essential, requiring the overcoming of existing limitations and the enhancement of their capabilities.

One of the most significant challenges faced by thin-shell structures is their extreme sensitivity to imperfections and external disturbances [5–8]. Even minor deviations from an ideal geometry can drastically reduce their load-bearing capacity, primarily by diminishing their resistance to buckling. This sensitivity complicates the prediction of the buckling behavior [3, 9], which stems from the minimal energy barrier between the pre-buckling and post-buckling states, where even infinitesimal perturbations can trigger early buckling [10, 11]. While traditional approaches rely on empirical stochastic methods to establish lower bounds (knockdown factors [12, 13]) for buckling loads, these methods face two critical limitations. First, the results are very conservative, leading to a reduction in structural mass efficiency. Second, they require extensive destructive testing, which limits scalability and applicability to complex geometries and materials [14].

While early work focused on predicting the buckling load, additional complications arise when trying to predict the post-buckling deformed shape. At the buckling point, the shell undergoes a highly nonlinear process driven by the interaction between global deformations, buckling eigenmodes and imperfections. This phenomenon, known as buckling localization [15, 16], produces a large number of energetically competing solutions (referred to as spatial chaos [17, 18]). Both energy barrier degradation and localization are highly imperfection-sensitive phenomena, which have

been shown to contribute to the unpredictability of the buckling behavior and are especially pronounced in structures with lower shell thicknesses [6, 19].

Recent advancements in understanding buckling stability have focused on energy barriers, which quantify the resistance to instability. A probing methodology was introduced to map stability landscapes, enabling the identification of the critical energy barriers driving disturbance sensitivity ("shock-sensitivity") in thin-shell structures [20–22]. Virot et al. [10] experimentally implemented the probing technique to cylindrical shells, indicating that the complex stability of shells can be reduced to a simpler, low-dimensional description. Marthelot et al. [23] demonstrated this technique on pressurized hemispherical shells, showcasing its ability to pinpoint imperfection-sensitive regions. These insights demonstrate that small amplitude disturbances can easily overcome the energy barrier and cause early buckling [18]. Royer and Pellegrino [3] extended these methods to ladder-type coilable structures, providing valuable insights into the stability of complex geometries. Further extension to probing-based stability analysis included applications to cylindrical [24–26] and spherical [27] shells, and circular arches [28], cylindrical shell roofs [29] and prestressed stayed columns [30].

While most probing studies focused on the sensitivity to disturbances, additional work showed that localized imperfections can significantly lower the energy barrier and therefore trigger early buckling [3, 11, 31]. The sensitivity of thin-shells to imperfections is strongly influenced by the severity and location of defects. Ning and Pellegrino [32] explored imperfection-insensitive designs for axially loaded thin-shell cylinders. Derveni et al. [33] demonstrated that the critical buckling strength of pressurized hemispherical shells with multiple defects is dictated by the most severe imperfection. Cervi and Virgin [34] conducted parametric studies on the effects of initial geometric imperfections on cylinder buckling, revealing variations in the buckling load and buckling mode shape. Similarly, Lee et al. [35] showed that strategically designed imperfections could enhance stability by redistributing stress and increasing resistance to buckling. These findings emphasize the importance of engineered imperfections as a tool to optimize buckling resistance, offering a systematic approach to enhancing the performance and reliability of thin-shell structures.

Besides probing, the influence of imperfections on the buckling behavior of shell structures has been extensively studied, with much of the existing research focusing on quantifying the reduction in buckling strength through the knockdown factor [33, 36–41]. However, effect of imperfection characteristics on the buckling energy barrier has not yet been quantitatively investigated. Early work by Hutchinson and Thompson [11] investigated the relationship between localized dimple imperfections and energy barrier in spherical shells, emphasizing the influence of dimple amplitude. This was later adapted by Royer and Pellegrino [3] to ladder-type coilable structures under bending, further highlighting the sensitivity of the buckling energy barrier to geometric imperfections. Expanding upon these studies, the present work employs the probing methodology to provide a deeper understanding of the link between imperfections and buckling energy barrier. We conduct a comprehensive numerical investigation that considers both positive (also refered to as "bumps" [39]) and negative dimples, examining how their location, amplitude, and width affect buckling

energy barrier. We focus here on open-section thin shells subjected to a bending moment. Key areas of focus include the variation of energy barriers, the propagation of localized buckle, and the comparative effects of positive and negative dimples on shell stability. The main objective of this methodology is to give a more thorough understanding of how to modulate the stability of thin-shell structures using localized "dominant" geometric imperfections.

The paper is structured as follows: Section III outlines the methodology, including the probing approach to computing the buckling energy barrier and its finite element implementation. Section IV presents results for both perfect and imperfect structures, focusing on energy barrier variations and buckle propagation.

III. Methodology

A. Probing the Buckling Energy Barrier

Figure 1 presents a schematic overview of the methodology, which consists of three main steps: (a) probing the buckling energy barrier, (b) identification of the critical buckling location, and (c) introduction of a localized geometric imperfection.

In the first step (Figure1a), a probing methodology is utilized to investigate the buckling stability of the structure. As the structure is subjected to a constant bending moment (M_y^0), the probing procedure applies a controlled localized displacement to the location of maximum buckling deformation. We create a stability landscape [10, 42] by gradually increasing the probe displacement (D_p) and measuring the reaction force (F_p) at the probing location, quantifying how sensitive the structure is to specific perturbations. This landscape highlights important characteristics, especially the point at which the reaction force drops to zero, signifying the onset of instability corresponding to the formation of a localized dimple [23]. The energy barrier required for the structure to change from a stable to an unstable buckled configuration is directly quantified by the work done by the probe to form this dimple [21]. In particular, unbuckled and unstable buckled equilibria are separated by a hump in the probe force-displacement characteristics, and the area under that hump corresponds to the buckling energy barrier [8]. This method enables the identification of the earliest load at which buckling can happen under disturbances, which is found earlier than the critical load obtained by a traditional linear bifurcation analysis, in addition to capturing the energy barrier [10]. In the second step (Figure 1b), the energy barrier is plotted as a function of the probe location. The minimum value corresponds to the location where an imperfection would have the greatest impact on local buckling. This critical location is then used to introduce a controlled imperfection.

In the third step (Figure1c), a localized geometric imperfection in the form of a Gaussian dimple is introduced at the identified critical location. The imperfect shell is then probed along its length to examine how this controlled imperfection alters the minimum buckling energy barrier. In particular, we hypothesize that this localized geometric imperfection could significantly alter the structure's stability characteristics and either postpone or accelerate the onset

of buckling.

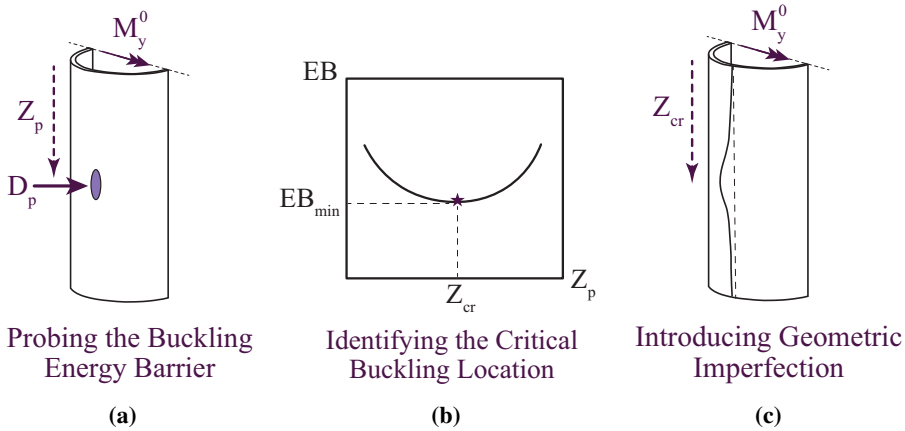


Fig. 1 Schematic representation of the methodology.

B. FEM Implementation

To investigate the buckling behavior of thin open shell structures using the probing methodology, a finite element model (FEM) is developed. This model is implemented in the Abaqus 2023 commercial software, utilizing Python scripting. Geometry inputs are provided in Table 1. The open-section shell is modeled with 4-node reduced integration shell elements (S4R) and finite strains. A schematic representation of the geometrical parameters, the boundary condition and the applied bending moment is shown in Figure 2. The structure is composed of a [0/90/0] carbon fiber reinforced polymer (CFRP, MR60H/PMT-F7) laminate. The stacking sequence is chosen such that it corresponds to physical prototypes manufacturable in the laboratory for an ongoing experimental validation campaign. This symmetric laminate minimizes residual thermal distortions during curing. Although alternative fiber orientations such as ±45° plies could modify the buckling response quantitatively, the overall behavior is primarily governed by geometry. Similar trends were observed in an earlier study employing a different material model [8], and therefore no qualitative changes in the buckling behavior are expected. The three-ply laminate is homogenized using Classical Lamination Theory implemented in the Abaqus composite module, and each ply is modeled as an orthotropic lamina with the a linear elastic material behavior. It is important to clarify here that all buckling phenomena examined in this study are purely elastic. The CFRP material properties [43] are summarized in Table 2.

Table 1 Shell geometric parameters.

Parameter	L (mm)	t (mm)	R (mm)	θ (deg)
Level	100	0.12	20	150

The simulation of the probing process is conducted in two non-linear static steps (Static general in Abaqus, Arclength solver). First, a preloading step is implemented to apply a bending moment on the structure. The bending is then kept

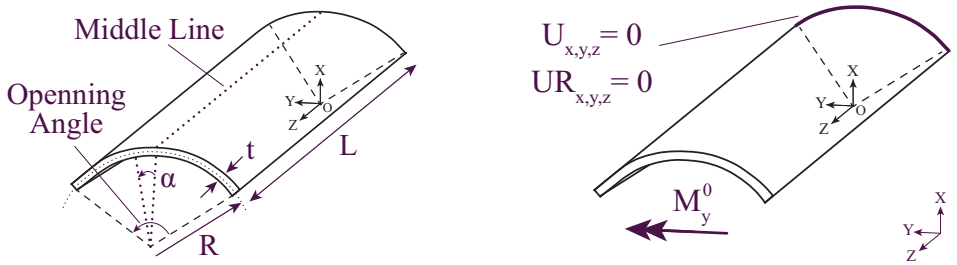


Fig. 2 Schematic of the (a) shell geometry, (b) boundary conditions, and applied bending moment.

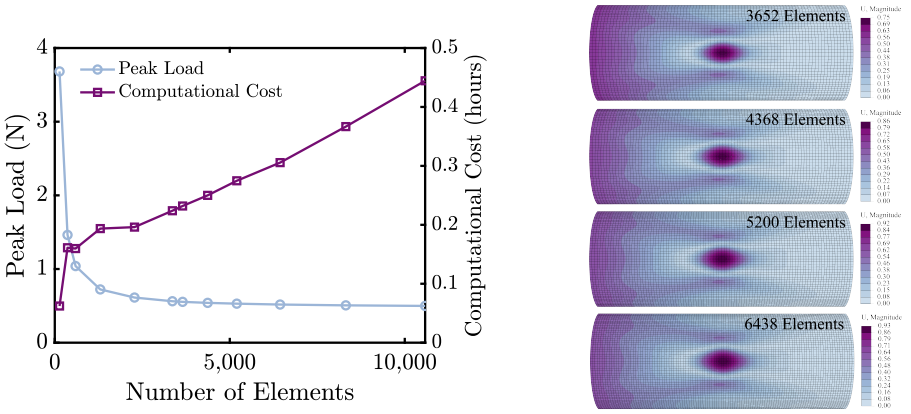
Table 2 Material properties of the composite lamina used in the study. [43]

Material	E_1 (GPa)	E_2 (GPa)	G_{12} (GPa)	ν_{12}	t (mm)
CFRP	174.40	8.39	6.40	0.259	0.04

constant following preloading, and a second analysis step is employed to perform probing. In this step, a localized radial displacement is applied to a single node on the shell surface, representing the action of a mechanical probe. The displacement is incrementally increased while recording the reaction force at the probe location to map out the shell's stability landscape. This process is repeated for a range of moments up to the linear buckling moment. In this procedure the only parameter varied is the applied bending moment, referred to as M_y^0, while all other parameters are kept constant. The linear critical buckling moment, M_{cr-lin}, is chosen as the upper limit to ensure that the structure remains in the prebuckling regime in the absence of probing. In practice, the load at which the bifurcation is encountered may vary from M_{cr-lin} and iteratively solving the eigenvalue problem as the preload is increased may yield more accurate predictions [44]. However, this study largely focuses on the buckling energy barrier at significantly lower loads than the bifurcation point, and therefore an accurate prediction of the bifurcation load is not critical.

A mesh convergence study is presented in Figure 3. Of particular importance is the sensitivity of the buckling localization phenomenon to mesh density, and numerical imperfections can in practice affect thin-shell buckling the same way geometric imperfections do. A probing analysis is conducted on the nominally perfect structure, for a probe location $Z_p = 54\ mm$ and $\alpha = 0^o$, as described in the previous paragraph. This test case corresponds to the analysis presented in Section IV.B.3, and probing is performed using an arclength solver (Riks in Abaqus). The peak force, which significantly affects the buckling energy barrier, and corresponding deformed shapes at the stable equilibrium location (location C, see Section IV.B.3) are compared for various mesh densities. A mesh consisting of 5, 200 elements is selected for the remainder of the study, which corresponds to a edge seed size of 1 mm. This mesh density lies in the plateau region of the convergence curve, where the variation in the peak load is minimal. This mesh density is selected due to the significant increase in computational cost with finer meshes, which makes the large number of simulations required in this study quickly intractable. While there exists a minimal variation in peak load between the

1 mm element size and finer meshes, this choice provides a practical balance between accuracy and computational efficiency. To assess the ability of the mesh to resolve the formation of local buckles, the corresponding deformed shapes at the stable equilibrium location for different mesh densities are illustrated in Figure 3b. The equilibrium location of maximum deformations remains at $Z = 50\ mm$ and the deformed shapes are consistent for all models with more than 3652 elements (seed size less than 1.2 mm).



(a) **(b)**

Fig. 3 Mesh convergence study for probing at $\alpha = 0^o$ and $Z_p = 54\ mm$, with the corresponding deformed shapes at the stable equilibrium location.

To investigate the effect of geometric imperfections on the buckling energy barrier, a localized dimple is introduced into the shell structure prior to the preloading step. The imperfect shell geometry is obtained by imposing a normal displacement fields on the shell surface which takes the shape of a Gaussian dimple

$$\omega = \delta e^{-\frac{(Z-Z_d)^2}{2\sigma^2}} \tag{1}$$

δ refers to the peak amplitude, where a positive value corresponds to an outward (positive) dimple and a negative value to an inward (negative) dimple. Z_d represents to the peak's coordinate along the length, and σ is the Gaussian standard deviation, which corresponds to the dimple width (Figure 4). Once the dimple is generated in the shell, the deformed geometry is then imported in the probing analysis described above.

IV. Results and Discussion

A. Linear Stability Predictions

A buckling eigenvalue analysis enables the computation of the linear buckling moment. This moment corresponds to the load at which a bifurcation is encountered on the prebuckling path. The corresponding buckling eigenmode corresponds to the deformed shape found on the post-buckling branch that arise from the bifurcation point. However, in practice, localized solutions dominate the buckling behavior in thin shell structures [8, 45–47]. These solutions cannot

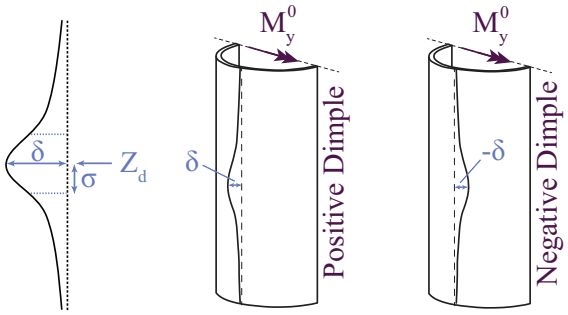


Fig. 4 Schematic representation of the Gaussian dimple geometric parameters and the profiles of the positive and negative dimples.

be found by an eigenvalue analysis because they never intersect the prebuckling path, despite running asymptotically close to it [48]. These localized solutions are critical in practice because they correspond to the lowest mountain pass points in the energy landscape [9] and are therefore easiest to reach when the buckling energy barrier is eroded by unavoidable imperfections present in real structures, as observed in experiments [47]. In this paper, the probing methodology [10, 42] is used to analyze these localized solutions, and these results are presented in the following sections.

However, a classical eigenvalue analysis was first performed on the perfect open-section thin-shell to determine the linear buckling moment and buckling eigenmode. While giving different critical loads and deformed shapes than the localized solutions, the linear stability analyses can help us understand localization, as described next. This analysis yields a linear buckling moment of $M_{cr-lin} = 3.0\ Nm$, and a linear buckling mode featuring a global distribution of inward and outward dimples as illustrated in Figure 5. It has been previously observed that the localization of buckling deformations can be related to the locations of maximum inward deformations in the buckling eigenmode [8].

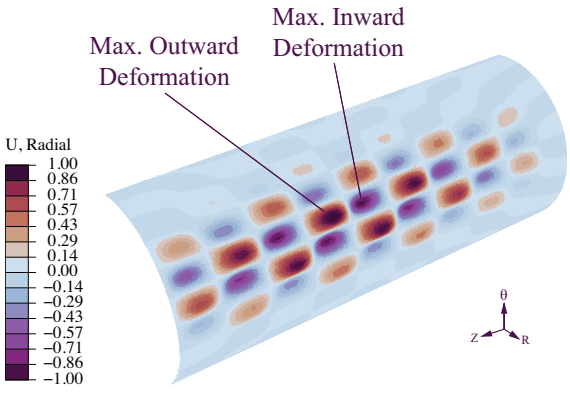


Fig. 5 Deformed shape obtained from a linear buckling analysis.

The location of maximum inward buckling deformation ($\alpha = 5^o, Z_{cr} = 54\ mm$), identified through the eigenvalue analysis, is critical (refer to Figure 2a for the geometric definition of α and the Z axis), and we expect localized solutions to be encountered first at this location, for a nominally perfect structure. However, due to the symmetry of the problem,

and the fact that only a single buckle is expected to appear first in practice, this critical location is likely to shift toward the center line of the structure ($\alpha = 0^o, Z_{cr} = 54\ mm$, 5-degree angular offset from the eigenmode's peak deformation). Therefore, we expect the buckling energy barrier of localized buckling solutions to be minimal at this location. This hypothesis will be verified in the next sections where probing is extended to the entire shell. Note that the eigenvalue analysis is not required to conduct the probing analysis, and it is only highlighted here as an interesting comparison.

B. Buckling Energy Barrier in Perfect Structure

1. Stability Landscape of Shell Buckling

Probing the critical buckling location identified in the previous section enables the acquisition of the stability landscape of shell buckling. Figure6 illustrates the stability landscape obtained by plotting the reaction force at the probe location as a function of the probe displacement for various levels of the main bending moment. In this figure, the black contour lines are cross-sections of the landscape at constant moments. The initial bending moment for these levels is determined based on the linear critical buckling moment (M_{cr-lin}), which is used as an upper bound. The moment is then gradually reduced in increments of 0.1 Nm until it reaches zero. Previous publications [3, 10, 42] comprehensively described the key details of the stability landscape. Although our structure differs from those in these studies, the landscape exhibits a similar topography. It highlights two key features: the minimally buckled state, which corresponds to the minimum load at which the probe force drops to zero, and the energy barrier to buckling. Buckling occurs when the probe force reaches zero, as indicated by the white dashed line in Figure6. For moments strictly below $M_y^0 = 1.4\ Nm$, the probe forces remain positive, indicating that no local buckle can form in the structure. $M_y^0 = 1.4\ Nm$ (the white solid curve in Figure6) corresponds to the minimally buckled state for which the probe force first drops to zero. Buckled equilibria exist for moments above M_y^0. Compared to M_{cr-lin}, the earliest possible transition into buckling occurs at a much lower moment owing to the structure's sensitivity to disturbances and imperfections. The energy barrier to buckling (EB), defined as the area under the force-displacement response curve (as illustrated in Figure 6), represents the minimum energy required to trigger early buckling in the structure. It is the key quantity of interest in this study and is monitored quantitatively, with a detailed discussion provided in the following section.

2. Energy Barrier Variation Across the Shell

In this section, we examine the variation of the buckling energy barrier across the shell by sequentially probing multiple locations. The main objective is to identify the location with the lowest energy barrier, which indicates where buckling is most likely to initiate. In addition to probing different locations on the middle line ($\alpha = 0^o$), lines with $\alpha = 2^o$ and $\alpha = 5^o$ angular offsets from the middle are also probed. The energy barrier as a function of the probe location for different moments is plotted in Figure 7. The relative variation in energy barrier at the critical location $Z_p = 50\ mm$ is computed as the difference between the maximum and minimum energy barrier values divided by the

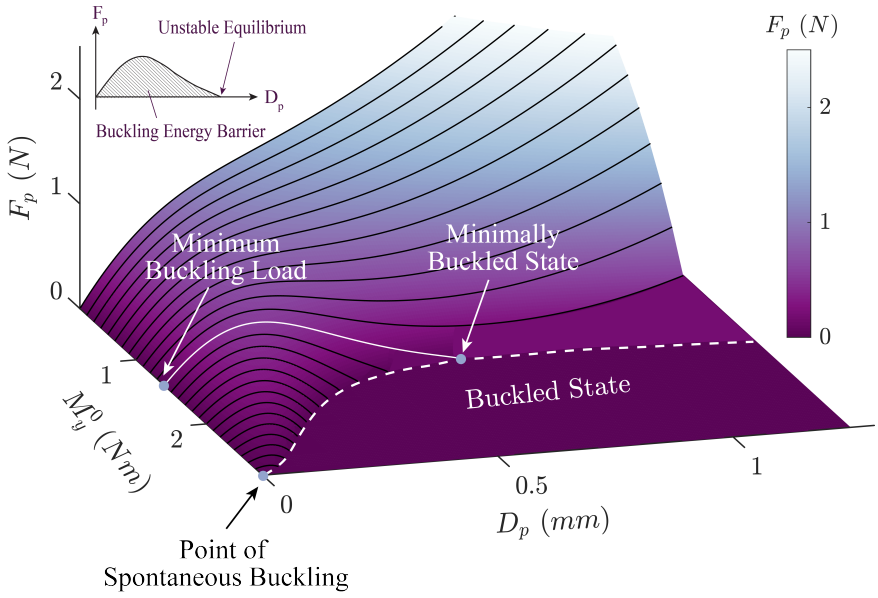
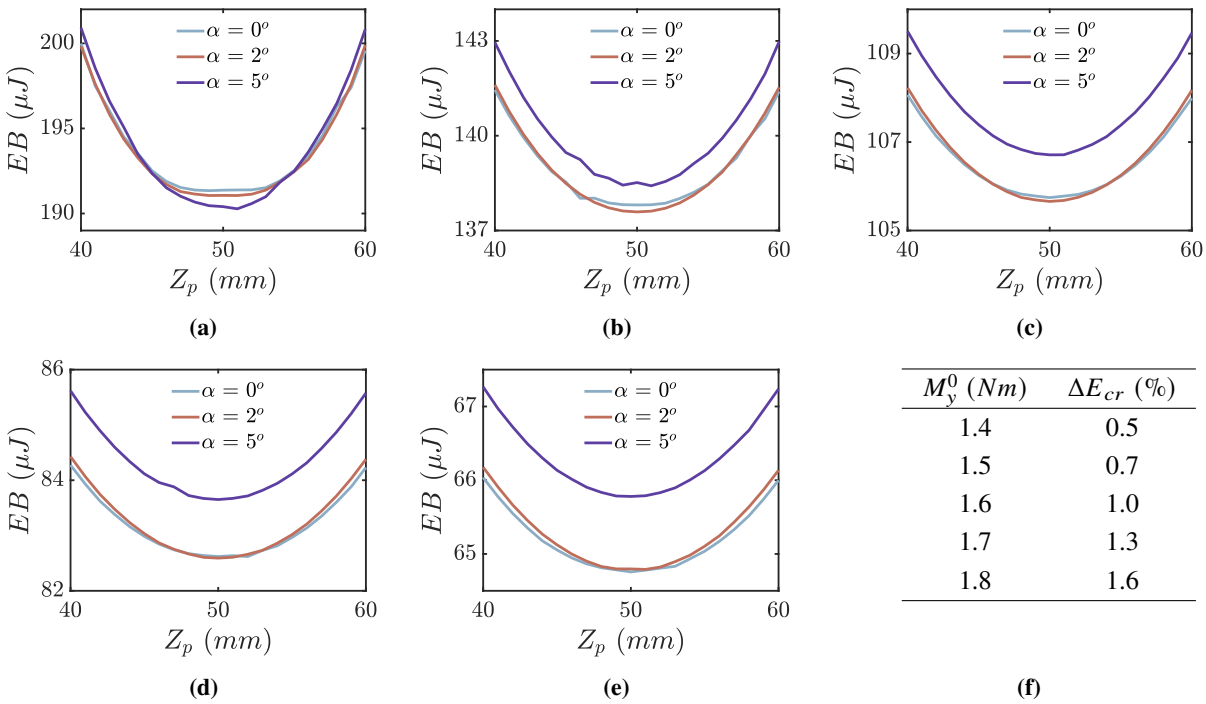


Fig. 6 Thin-shell buckling stability landscape.

minimum value. For $M_y^0 = 1.4\ Nm$, the energy barrier variations across all α values are minimal, with a maximum difference of only 0.5%. As the moment increases, the energy barrier difference widens to 0.7% for $M_y^0 = 1.5\ Nm$ and to 1.6% for $M_y^0 = 1.8\ Nm$. This observation indicates that a critical buckling location emerges as the moment increases, and buckling at other locations becomes less and less likely. The lowest energy barrier is observed at the location of $\alpha = 0^o$ and $Z = 50\ mm$, indicating the most probable location for buckling initiation as the applied moment increases.

3. Buckle Propagation

The previous section discussed the energy barrier variation to initiate buckling. However, the buckling initiation location does not always correspond to the location at which the buckle is found in equilibrium. Figure 8 presents the force-displacement curve for probing at $\alpha = 0^o$ and $Z = 54\ mm$. The characteristic is initially well behaved but quickly encounters an instability at a probe displacement around $D_p = 0.6\ mm$, which results in a vertical tangent and a loss of convergence of the Newton-Raphson solver. The analysis is extended beyond this instability by employing an arclength solver (modified Riks method in Abaqus). Note that the Newton–Raphson solver is initially used to reduce computational cost, and the Riks solver is only used for cases where instabilities are encountered under displacement control. The two solvers yield identical results up to the point where a vertical tangent is encountered. Examination of the probe characteristic post-instability reveals that the unstable path physically corresponds to buckle propagation. Buckle propagation is characterized by inherent instability, which serves as the defining signature of this phenomenon. As can be seen in Figure 8, after the initiation of buckling at the probe location (point A), the buckle propagates longitudinally to the location corresponding to $Z = 46\ mm$ (point B), and ultimately stabilizes at $Z = 50\ mm$ (point C) where it remains in equilibrium. This finding demonstrates that the location where buckling initiates may differ from



$M_y^0\ (Nm)$	$\Delta E_{cr}\ (\%)$
1.4	0.5
1.5	0.7
1.6	1.0
1.7	1.3
1.8	1.6

(f)

Fig. 7 Energy barrier across the length: (a) 1.4 Nm**, (b)** 1.5 Nm**, (c)** 1.6 Nm**, (d)** 1.7 Nm**, (e)** 1.8 Nm**, (f) Relative energy barrier variation at** $Z_p = 50\ mm$**.**

the location where the structure ultimately stabilizes in the post-buckling regime. Previous research has demonstrated comparable trends [3]. Furthermore, probing locations offset from the middle line ($\alpha \neq 0^o$) revealed that, in addition to propagating longitudinally, the buckle also moves transversely toward the middle line. For all the probing locations, the buckle tends to shift toward the middle line and stabilize at $Z = 50\ mm$ in the stable equilibrium state.

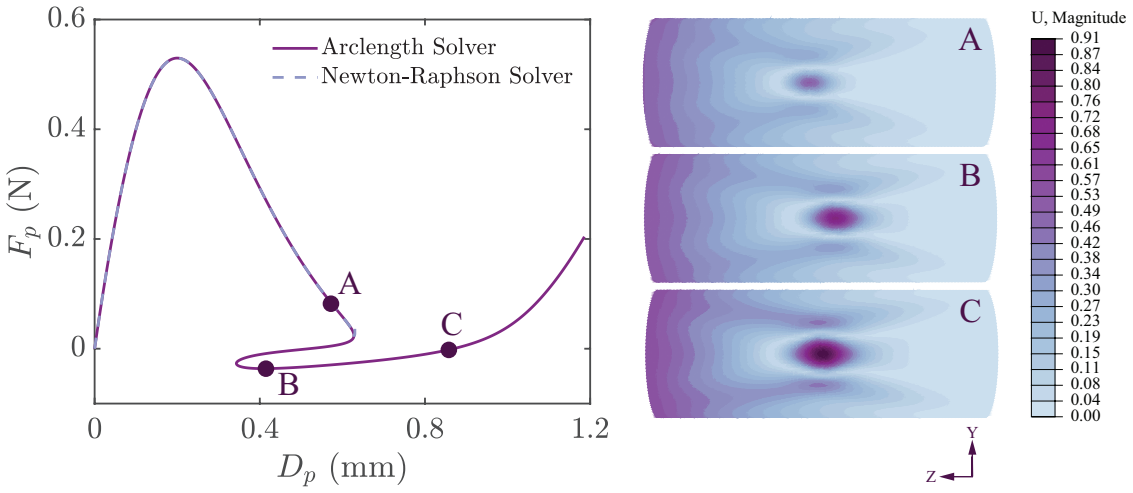


Fig. 8 Force-displacement curve for probing at $\alpha = 0^o$ **and** $Z_p = 54\ mm$**, with the corresponding deformed shapes illustrating buckling initiation and propagation.**

C. Influence of Geometric Imperfections on Buckling Stability

1. Characterization and Implementation of Structural Imperfections

To understand and quantify how geometric imperfections influence shell buckling, the impact of a localized single dimple imperfection incorporated into the initial shell geometry is investigated through probing methodology. The selection of a dimple as the geometric imperfection is based on recent research [9], which demonstrates that buckling onset consistently coincides with the formation of a single dimple deformation. This deformation is identified as the lowest energy path to buckling, making it the critical geometric imperfection [9].

As the sensitivity of thin-shells to imperfections is strongly influenced by the location of defects, first, we determine the location of the dimple. Locations with the lowest energy barrier are prioritized when selecting the dimple location, as introducing an imperfection at these points is expected to have the most significant impact on the shell's global buckling behavior. Linear theory (discussed in section IV.A) identifies $Z = 54\ mm$ as the critical buckling location, corresponding to the maximum inward deformation point. However, $Z = 50\ mm$ might also be regarded as a critical point, given the location of the minimum energy barrier to buckling and the stabilized buckle in the buckled equilibria (discussed in sections IV.B.2 and IV.B.3). Accordingly, the location of $\alpha = 0^o$ and $Z_d = 50\ mm$ is selected as the critical location for the dimple placement, which corresponds to the dimple's peak coordinate in equation 1. To introduce dimple imperfection into the shell, both positive dimples ($\delta > 0$) and negative dimples ($\delta < 0$) are analyzed. The amplitude of dimples varies between 10 and 150 μm, and the dimple width (σ) is selected in the range of 1 to 10 mm.

2. Impact of Imperfection amplitude on Buckling Energy Barrier

Thin-shells are extremely sensitive to imperfections, which significantly affect their buckling behavior. This effect is investigated by introducing a localized dimple at the critical buckling location ($Z_d = 50\ mm$) and analyzing the variation of the buckling energy barrier at that point ($Z_p = 50\ mm$) for various dimple amplitudes. Figure 9 compares the buckling energy barrier of the perfect and imperfect structures with a fixed normalized imperfection width of $\sigma/L = 0.07$.

The perfect structure's buckling energy barrier decreases as the applied moment increases. This implies that the structure gradually loses stability as the main loading rises, requiring less energy to transition into a buckled state. This stability is affected by introducing positive and negative dimples, as indicated by the variations in EB for different δ/t values.

When the introduced imperfection is a positive dimple, as depicted in Figure 9a, the buckling energy barrier is increased in comparison to the perfect structure, thereby enhancing stability. Increases in the imperfection amplitude lead to higher energy barriers. However, at higher amplitudes ($\delta/t > 0.5$), the energy barrier suddenly drops to zero when the main loading is increased. For instance, the energy barrier of the dimple with an amplitude of $\delta/t = 0.92$ drops to zero at the moment of 2 Nm. This behavior indicates the presence of a critical threshold, beyond which the positive dimple not only fails to improve buckling resistance but also compromises the structural integrity. We hypothesize that

this is because, once the critical amplitude threshold is surpassed, the buckle is forced to initiate at a different point than the probe location. High-amplitude dimples redistribute stress and shift the critical buckling location where buckling initiates. The shift of the critical buckling location is demonstrated in section IV.C.3. Larger dimples, therefore, cause the structure to be more prone to collapse even without external disturbances.

When negative dimples are defined, Figure (9b), the perfect structure maintains the highest energy barrier, requiring the most energy to initiate buckling compared to the imperfect shells with negative dimples. Negative imperfections erode the energy barrier, making buckling more probable. As δ/t increases, the energy barrier progressively reduces, demonstrating that imperfections facilitate earlier buckling initiation by lowering the required energy input. Increasing the imperfection amplitude reduces the buckling energy barrier further. For larger values of amplitude ($\delta/t > 0.08$), the moment at which buckling occurs without disturbances ($EB = 0$) is reduced compared to the perfect structure. This moment, referred to as the point of spontaneous buckling [10], represents the transition of the structure into its post-buckling regime without any external disturbance [3]. For a perfect structure, this point occurs at $M_y^0 = 2.8\ Nm$ (Figure 6), whereas for an imperfect structure with a negative dimple characterized by $\delta/t = 0.25$, the moment of spontaneous buckling decreases to $M = 1.8\ Nm$.

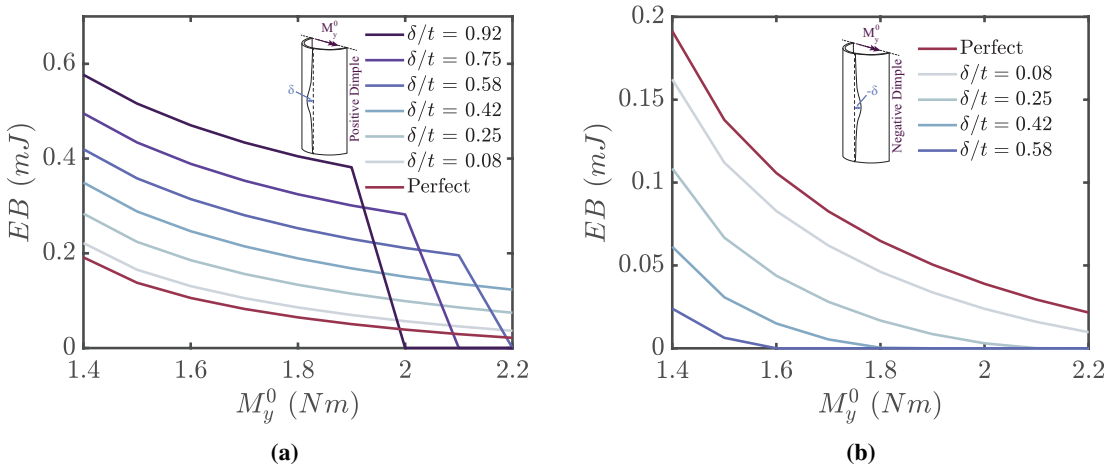
These findings suggest that even minor imperfections can significantly impact the stability of thin shells. They present a practical strategy for tailoring buckling resistance in thin-shell structures. This can be achieved by carefully introducing dimples with controlled sizes:

- Enhance stability by defining positive dimples with smaller amplitudes, which can raise the buckling energy barrier.
- Trigger controlled collapse in structures intended to undergo programmed buckling by defining dimples with larger amplitudes.

Such understandings can influence the design of customized structures and metastable shells, enabling imperfections to be adapted into advantages that enhance engineering performance. While the conclusions drawn here are based on the specific structure and loading conditions examined in this study, we hypothesize that these findings are more general, based on observations in other structures [10, 11]. This hypothesis will be verified in future work.

3. Impact of Imperfection width on Buckling Energy Barrier

The previous section investigated the effects of imperfection amplitude by introducing both positive and negative dimples. This section examines the impact of imperfection width, focusing only on the positive dimple. A localized dimple is introduced at the $Z_d = 50\ mm$ and $Z_d = 54\ mm$ locations, and the energy barrier variation is analyzed at those locations for different dimple amplitudes and widths, under a specific value of moment $My^0 = 1.4\ Nm$ (the minimum buckling load, Figure 6). It should be noted that the probe is applied at the dimple location, meaning that measurements of the energy barrier are taken directly at the point where the imperfection is introduced. Figure 10a shows how the



(a) **(b)**

Fig. 9 Effect of imperfection amplitude on the buckling energy barrier ($\sigma/L = 0.07$, $Z_d = Z_p = 50\ mm$): (a) positive dimple, (b) negative dimple.

variation of dimple width affects the buckling energy barrier for $Z_d = 50\ mm$. The effect of the dimple amplitude is consistent with previous findings in IV.C.2.

Examining the influence of dimple width, it is observed that for small imperfection amplitudes ($\delta/t < 0.5$), the energy barrier increases moderately with the dimple width, and no sudden slope changes are observed. The energy barrier eventually plateaus for larger values of width, indicating that, at lower amplitudes, the imperfection width does not affect the buckling behavior.

For higher dimple amplitudes $\delta/t > 0.5$, three distinct regimes can be identified based on the response of the energy barrier to increasing imperfection width. These regimes are shown in Figure 10b for $\delta/t = 0.75$, with the corresponding probe force vs probe displacement overlaid on the energy barrier graph for each regime.

In the first regime, corresponding to the smaller σ/L values ($\sigma/L < 0.04$), the energy barrier increases gradually as the imperfection width increases. In this regime, under displacement control, the force–displacement curve (Figure 10b, inset: $\sigma/L = 0.01$) remains stable up to the unstable equilibrium point (purple dot in Figure 10b).

As the imperfection width increases beyond a critical threshold ($\sigma/L = 0.04$ for $\delta/t = 0.75$), the structure transitions into the second regime, where the energy barrier reaches a plateau, indicating that the width of the dimple does not affect the buckling response in this region. The force–displacement curve for this regime (Figure 10b, inset: $\sigma/L = 0.05$) exhibits a snap through behavior, where the probe characteristic becomes unstable under displacement control. This behavior results from buckle propagation, i.e., the shifting of the buckling location along the structure's length. As in regime 1, the probe force reaches negative values, indicating buckling, but the arclength solver is now able to locate the stable equilibrium (blue dot in Figure 10b).

In the third regime, corresponding to the highest σ/L values, no buckled equilibria exist and the energy barrier is therefore undefined. The $F_p - D_p$ curve for this regime (Figure 10b, inset: $\sigma/L = 0.10$) shows a local minimum of

force but does not drop below zero. This observation implies that beyond a critical imperfection width, the dimple has effectively altered the buckling behavior, preventing the formation of post-buckling equilibria, thus suppressing the potential for early buckling for this specific value of moment. This highlights that beyond modulating the buckling energy barrier, positive dimple imperfections can also be used as a mechanism to adjust the minimum buckling load, and therefore the range of moments for which the structure is metastable pre-buckling. A qualitative study indicated that this specific imperfection width ($\sigma/L = 0.07$) is close to the width of a natural buckle that would form in the perfect structure for this specific value of moment. However, further research is required to investigate the reason behind this particular value of σ/L.

When introducing a dimple at a non-critical location ($Z_d = 54\ mm$), as shown in Figure 11, the energy barrier exhibits similar trends but with a transition to the third regime for lower values of dimple width. This occurs because buckling is less likely initiate at a non-critical location, and therefore can be suppressed by a broader range of imperfection characteristics.

From the dimple width analysis, it can be concluded that highly localized positive dimples may have a limited impact on stability. In contrast, their impact on buckling is significant beyond a critical width. It suggests potential strategies for imperfection insensitive designs where imperfections can be used to tune the buckling behavior of thin-shells and prevent premature failure.

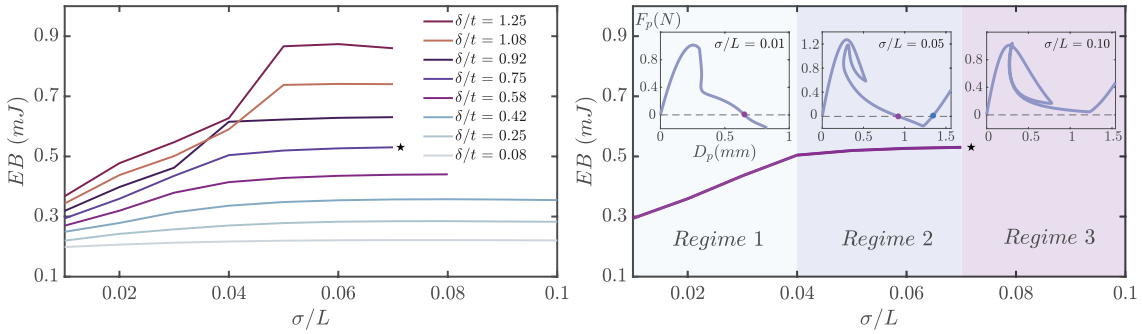


Fig. 10 (a) Effect of imperfection width on the buckling energy barrier for a positive dimple ($Z_d = Z_p = 50\ mm$, $M_y^0 = 1.4\ Nm$), (b) $\delta/t = 0.75$. Insets: probe force vs. probe displacement.

4. Spatial Extent of Imperfection Influence on Buckling

In sections IV.C.2 and IV.C.3, the probe location and the dimple location were identical, meaning that measurements of the energy barrier were taken directly at the point where the imperfection was introduced. In this section, the dimple is placed at the critical location ($Z_d = 50\ mm$), and the entire length of the structure is probed ($0 \leq Z_p \leq 100\ mm$) to determine the spatial extent of the dimple's effect on the energy barrier. This approach allows for a more comprehensive understanding of how a localized imperfection affects the global buckling behavior of the shell. Figure 12a presents the

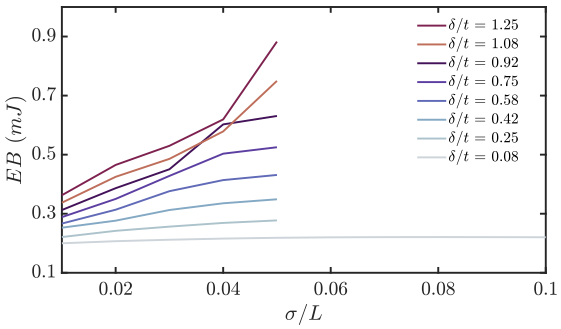


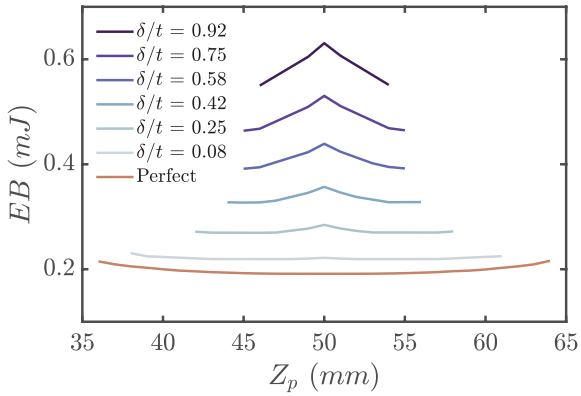
Fig. 11 Effect of the imperfection width on the energy barrier for a positive dimple at $Z_d = Z_p = 54\ mm$, subjected to a moment $M_y^0 = 1.4\ Nm$.

effect of a positive dimple on the buckling energy barrier along the shell length, for $\sigma/L = 0.07$. The regions in the figure where no data points are present indicate that there is no buckling energy barrier and no buckled equilibria exist at those Z locations, for that specific moment.

Comparing the perfect shell with the dimpled cases, it is evident that by introducing a localized imperfection the range of locations for which buckled equilibria can be found shortens. It means that the minimum buckling load required for triggering early buckling increases in those locations, compared to the perfect structure. This result further confirms that the dimple can act as a stabilizing feature, delaying the onset of the shell's disturbance-sensitive (also called shock-sensitive) regime.

For the perfect structure, the energy barrier remains relatively low and uniform across the shell length. Examining the range of locations at which buckling can be initiated (length of the buckling sensitive region) in the absence of imperfections, no buckled equilibria can be found for Z values lower than 36 mm and higher than 64 mm, indicating that buckling can only be initiated within the region $Z = 36 - 64\ mm$. It is worth noting that while buckling is initiated within this region, the location at which the buckle is found in equilibrium may differ from the initiation location but still remains within this same Z range. This means 29% of the perfect structure's length can undergo local buckling. When a dimple is introduced, the buckling region narrows significantly as the imperfection amplitude increases. For small dimple amplitudes ($\delta/t = 0.08$), buckling still occurs over a substantial portion of the structure but is already reduced to 24% of its length. As the amplitude increases further, the length of the buckling sensitive region continues to decrease until it plateaus at approximately 11% of the structure length for amplitudes of $\delta/t > 0.5$. For the highest imperfection amplitude studied ($\delta/t = 0.92$), the sensitive length is minimal at 9% of L. This trend suggests that as the imperfection amplitude increases, the structure becomes significantly resistant to buckling over a significant portion of its length, effectively suppressing the potential for local buckling outside of a localized region. Therefore, we hypothesize that the location at which local buckling may be found in practice for these imperfect structures becomes more and more deterministic and less prone to what has been referred to as spatial chaos ([18]). The trend of energy barrier variation is

consistent with Figure 10; however, the energy barrier features a peak at the dimple location and decreases to form two local minima on either side of the dimple. This impact is more noticeable at higher amplitudes, indicating that larger dimples create localized regions with higher energy barriers.



(a)

δ/t	Length of the buckling sensitive region (% L)
Perfect	29
0.08	24
0.25	17
0.42	13
0.58	11
0.75	11
0.92	9

(b)

Fig. 12 (a) Influence of the imperfection on the energy barrier along the shell length ($M_y^0 = 1.4\ Nm$, $\sigma/L = 0.07$), (b) length of the region sensitive to local buckling.

5. Influence of imperfection on Buckle Propagation

After discussing the impact of imperfection amplitude and width on the buckling energy barrier in the previous sections, this section focuses on how imperfections affect the propagation of buckles. Figure 13 presents the probe force-displacement response of an imperfect shell under probing at $\alpha = 0^o$, $Z_p = 50\ mm$, subjected to a bending moment of $M_y^0 = 1.4\ Nm$). A positive dimple imperfection characterized by $\delta/t = 0.92$ and $\sigma/L = 0.07$ is introduced at $Z_d = 50\ mm$. Three key points along the probing path (A, B, and C) are highlighted on the curve. The corresponding deformed shapes illustrate how the buckle location varies during probing. The horizontal arrows (particularly in B and C) indicate the propagation direction of the buckle along the shell's longitudinal axis (Z-direction).

The probing path follows a stable increase and decrease in probe force, resulting in a buckle forming at the probe location ($Z_p = 50\ mm$). At point A, the probing characteristic encounters an instability characterized by a snap-through response of the structure, which physically corresponds to the propagation of the buckle along the shell's longitudinal axis (Z-direction) [8]. Following the onset of instability at point A, the structure experiences a snap-back behavior in the force-displacement response, where the probe displacement abruptly decreases from $D_p = 0.66\ mm$ (point A) to $D_p = 0.34\ mm$ (between point A and B). This sudden reduction corresponds to a snap-through event in which the buckle, initially concentrated at the probe location, begins to shift away from the probe location. In the deformed shape labeled B, the horizontal arrow illustrates the direction of this buckle migration, indicating that the localized deformation propagates away from the probe position and toward the fixed boundary condition along the shell's length. Then by

increasing the probe displacement, at point B, while the initial buckle exists at a non-probe location ($Z = 38\ mm$), a new buckle attempts to form at the probe location. This secondary buckling attempt is visible in the deformed shape labeled B, where two buckle locations are apparent, the initial one at $Z = 38\ mm$ and another at the probe location ($Z_p = 50\ mm$).

Although the probe force-displacement curve in Figure 13 displays self-intersections, the structure does not encounter multiple branches at these points. Looking at a higher order equilibrium manifold reveals that these intersections only exist in the probe force-displacement plane. For instance, on a surface created by the probe force, probe displacement, and bending rotation, the "intersections" found in the probe force-displacement plane yield two distinct equilibrium states with different bending rotation values. A similar behavior was previously observed in [8].

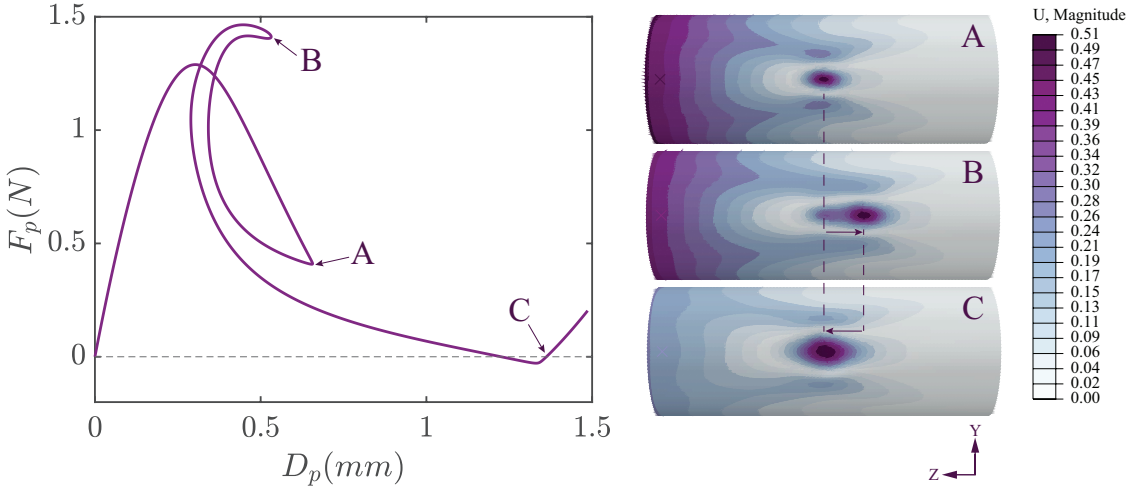


Fig. 13 Force-displacement response of an imperfect shell ($\alpha = 0^o$, $Z_p = 50\ mm$, $M_y^0 = 1.4\ Nm$) with a positive dimple ($\delta/t = 0.92$ and $\sigma/L = 0.07$) at $Z_d = 50\ mm$.

Comparing this behavior with the perfect shell (see Figure 8), it is evident that the imperfection alters the buckle propagation. In the perfect case, the buckle freely translates along the shell without resistance, and no attempt at forming a second buckle is observed. In contrast, the dimple in the imperfect shell acts as a local obstruction, partially resisting the buckle propagation back to the probe location and encouraging the formation of a secondary buckle at the probe location. However, due to the relatively moderate severity of the imperfection, characterized by $\delta/t = 0.92$ and $\sigma/L = 0.07$, this repulsion is not strong enough to permanently pin the primary buckle away from the probe location. Hence, from point B forward, the buckle gradually shifts back toward the probe location. Finally, at point C, the structure reaches a stable equilibrium with the primary buckle fully relocated to the probe location ($Z_p = 50\ mm$), as shown in the deformed shape labeled C.

V. Conclusion

The influence of the dimple imperfections on the buckling energy barrier and buckle propagation of open-section thin-shell structures is comprehensively investigated in this work. The findings showed that the stability and buckling response are significantly affected by the dimple imperfections' amplitude and width. Positive dimples generally raised the energy barrier, enhancing stability compared to the perfect structure. Conversely, negative dimples lower the load at which the structure spontaneously buckles. The study also reveals three different regimes that control how imperfection width affects the buckling behavior, emphasizing the existence of a critical width beyond which no buckled equilibria exist. It means that the minimum buckling load required to form buckles from perturbations increases. This result further confirms that the positive dimple acts as a stabilizing feature, delaying the onset of buckling. These Findings advance our knowledge of imperfection sensitivity in thin-shell structures and offer practical insights into designing multistable continuous shells and imperfection-insensitive structures. Ongoing research is working on experimentally validating these results, and future research will focus on engineering other types of "dominant imperfections" shells to fully control their buckling stability landscape.

Acknowledgments

The authors acknowledge internal funding from the College of Engineering at Cornell University.

References

[1] Royer, F., Zhang, J. Z., Overby, K., Zhu, E. Y., Bhundiya, H., Lang, J., and Cordero, Z. C., "Electrostatically Actuated Thin-Shell Space Structures," *AIAA SCITECH 2023 Forum*, 2023, p. 1302. https://doi.org/https://doi.org/10.2514/6.2023-1302.

[2] Arya, M., Lee, N., and Pellegrino, S., "Ultralight structures for space solar power satellites," *3rd AIAA Spacecraft Structures Conference*, 2016, p. 1950. https://doi.org/https://doi.org/10.2514/6.2016-1950.

[3] Royer, F., and Pellegrino, S., "Probing the stability of ladder-type coilable space structures," *AIAA Journal*, Vol. 60, No. 4, 2022, pp. 2000–2012. https://doi.org/https://doi.org/10.2514/1.J060820.

[4] Hasanyan, A. D., and Pellegrino, S., "Modeling of Damage in Coilable Composite Shell Structures," *AIAA Scitech 2023 Forum*, 2023, p. 0364. https://doi.org/https://doi.org/10.2514/6.2023-0364.

[5] Koiter, W. T., *On the stability of elastic equilibrium*, National Aeronautics and Space Administration, 1967.

[6] Donnell, L., and Wan, C., "Effect of imperfections on buckling of thin cylinders and columns under axial compression," *Journal of Applied Mechanics*, Vol. 17, No. 1, 1950, pp. 73–83. https://doi.org/https://doi.org/10.1115/1.4010060.

[7] Babcock, C. D., "The buckling of cylindrical shells with an initial imperfection under axial compression loading," Ph.D. thesis, California Institute of Technology, 1962.

[8] Royer, F., Hutchinson, J. W., and Pellegrino, S., "Probing the stability of thin-shell space structures under bending," *International Journal of Solids and Structures*, Vol. 257, No. May, 2022, p. 111806. https://doi.org/https://doi.org/10.1016/j.ijsolstr.2022.111806.

[9] Horák, J., Lord, G. J., and Peletier, M. A., "Cylinder Buckling: The Mountain Pass as an Organizing Center," *SIAM Journal on Applied Mathematics*, Vol. 66, No. 5, 2006, pp. 1793–1824. https://doi.org/https://doi.org/10.1137/050635778.

[10] Virot, E., Kreilos, T., Schneider, T. M., and Rubinstein, S. M., "Stability Landscape of Shell Buckling," *Physical Review Letters*, Vol. 119, No. 22, 2017, pp. 1–5. https://doi.org/https://doi.org/10.1103/PhysRevLett.119.224101.

[11] Hutchinson, J. W., and Thompson, J. M. T., "Imperfections and energy barriers in shell buckling," *International Journal of Solids and Structures*, Vol. 148, 2018, pp. 157–168. https://doi.org/https://doi.org/10.1016/j.ijsolstr.2018.01.030.

[12] Hilburger, M., "Developing the next generation shell buckling design factors and technologies," *53rd AIAA/ASME/ASCE/AHS/ASC structures, structural dynamics and materials conference 20th AIAA/ASME/AHS adaptive structures conference 14th AIAA*, 2012, p. 1686. https://doi.org/https://doi.org/10.2514/6.2012-1686.

[13] Weingarten, V. I., Seide, P., and Peterson, J. P., "Buckling of thin-walled circular cylinders," Tech. rep., NASA, 1968.

[14] Tzortzinis, G., Ai, C., Breña, S. F., and Gerasimidis, S., "Using 3D laser scanning for estimating the capacity of corroded steel bridge girders: Experiments, computations and analytical solutions," *Engineering Structures*, Vol. 265, 2022, p. 114407. https://doi.org/https://doi.org/10.1016/j.engstruct.2022.114407.

[15] Hutchinson, J. W., "Buckling of spherical shells revisited," *Proceedings of the Royal Society A: Mathematical, Physical and Engineering Sciences*, Vol. 472, No. 2195, 2016, p. 20160577. https://doi.org/https://doi.org/10.1098/rspa.2016.0577.

[16] Hunt, G. W., and Neto, E. L., "Localized buckling in long axially-loaded cylindrical shells," *Journal of the Mechanics and Physics of Solids*, Vol. 39, No. 7, 1991, pp. 881–894. https://doi.org/https://doi.org/10.1016/0022-5096(91)90010-L.

[17] Thompson, J., and Virgin, L., "Spatial chaos and localization phenomena in nonlinear elasticity," *Physics Letters A*, Vol. 126, No. 8-9, 1988, pp. 491–496. https://doi.org/https://doi.org/10.1016/0375-9601(88)90045-X.

[18] Groh, R. M., and Pirrera, A., "Spatial chaos as a governing factor for imperfection sensitivity in shell buckling," *Physical Review E*, Vol. 100, No. 3, 2019, p. 032205. https://doi.org/https://doi.org/10.1103/PhysRevE.100.032205.

[19] Koiter, W., "The effect of axisymmetric imperfections on the buckling of cylindrical shells under axial compression," *Mechanics*, 1963, pp. 265–279. https://doi.org/https://doi.org/10.2514/3.6123.

[20] Thompson, J. M. T., "Advances in shell buckling: Theory and experiments," *International Journal of Bifurcation and Chaos*, Vol. 25, No. 01, 2015, p. 1530001. https://doi.org/https://doi.org/10.1142/S0218127415300013.

[21] Thompson, J. M. T., and Sieber, J., "Shock-sensitivity in shell-like structures: with simulations of spherical shell buckling," *International Journal of Bifurcation and Chaos*, Vol. 26, No. 02, 2016, p. 1630003. https://doi.org/https://doi.org/10.1142/S0218127416300032.

[22] Hutchinson, J. W., and Thompson, J. M. T., "Nonlinear buckling interaction for spherical shells subject to pressure and probing forces," *Journal of Applied Mechanics*, Vol. 84, No. 6, 2017, p. 061001. https://doi.org/https://doi.org/10.1115/1.4036355.

[23] Marthelot, J., López Jiménez, F., Lee, A., Hutchinson, J. W., and Reis, P. M., "Buckling of a pressurized hemispherical shell subjected to a probing force," *Journal of Applied Mechanics*, Vol. 84, No. 12, 2017, p. 121005. https://doi.org/https://doi.org/10.1115/1.4038063.

[24] Yadav, K. K., Cuccia, N. L., Virot, E., Rubinstein, S. M., and Gerasimidis, S., "A nondestructive technique for the evaluation of thin cylindrical shells' axial buckling capacity," *Journal of Applied Mechanics*, Vol. 88, No. 5, 2021, p. 051003. https://doi.org/https://doi.org/10.1115/1.4049806.

[25] Abramian, A., Virot, E., Lozano, E., Rubinstein, S. M., and Schneider, T. M., "Nondestructive prediction of the buckling load of imperfect shells," *Physical Review Letters*, Vol. 125, No. 22, 2020, p. 225504. https://doi.org/https://doi.org/10.1103/PhysRevLett.125.225504.

[26] Cuccia, N. L., Kumar Yadav, K., Serlin, M., Virot, E., Gerasimidis, S., and Rubinstein, S. M., "Hitting the mark: probing at the initiation site allows for accurate prediction of a thin shell's buckling load," *Philosophical Transactions of the Royal Society A*, Vol. 381, No. 2244, 2023, p. 20220036. https://doi.org/https://doi.org/10.1098/rsta.2022.0036.

[27] Abbasi, A., Yan, D., and Reis, P. M., "Probing the buckling of pressurized spherical shells," *Journal of the Mechanics and Physics of Solids*, Vol. 155, 2021, p. 104545. https://doi.org/https://doi.org/10.1016/j.jmps.2021.104545.

[28] Shen, J., Groh, R., Schenk, M., and Pirrera, A., "Experimental path-following of equilibria using Newton's method. Part I: Theory, modelling, experiments," *International Journal of Solids and Structures*, Vol. 210, 2021, pp. 203–223. https://doi.org/https://doi.org/10.1016/j.ijsolstr.2020.11.037.

[29] Shen, J., Groh, R., Schenk, M., and Pirrera, A., "Experimental path-following of equilibria using Newton's method. Part II: applications and outlook," *International Journal of Solids and Structures*, Vol. 213, 2021, pp. 25–40. https://doi.org/https://doi.org/10.1016/j.ijsolstr.2020.11.038.

[30] Shen, J., Groh, R. M., Wadee, M. A., Schenk, M., and Pirrera, A., "Probing the stability landscape of prestressed stayed columns susceptible to mode interaction," *Engineering Structures*, Vol. 251, 2022, p. 113465. https://doi.org/https://doi.org/10.1016/j.engstruct.2021.113465.

[31] Sieber, J., Hutchinson, J. W., and Thompson, J. M. T., "Nonlinear dynamics of spherical shells buckling under step pressure," *Proceedings of the Royal Society A*, Vol. 475, No. 2223, 2019, p. 20180884. https://doi.org/https://doi.org/10.1098/rspa.2018.0884.

[32] Ning, X., and Pellegrino, S., "Experiments on imperfection insensitive axially loaded cylindrical shells," *International Journal of Solids and Structures*, Vol. 115, 2017, pp. 73–86. https://doi.org/https://doi.org/10.1016/j.ijsolstr.2017.02.028.

[33] Derveni, F., Choquart, F., Abbasi, A., Yan, D., and Reis, P. M., "The most severe imperfection governs the buckling strength of pressurized multi-defect hemispherical shells," *arXiv preprint arXiv:2410.08973*, 2024. https://doi.org/https://doi.org/10.1016/j.mechmat.2025.105295.

[34] Cervi, C., and Virgin, L., "An experimental parametric study assessing the effect of a certain initial geometric imperfection on cylinder buckling," *Aerospace Science and Technology*, Vol. 152, 2024, p. 109355. https://doi.org/https://doi.org/10.1016/j.ast.2024.109355.

[35] Lee, A., López Jiménez, F., Marthelot, J., Hutchinson, J. W., and Reis, P. M., "The geometric role of precisely engineered imperfections on the critical buckling load of spherical elastic shells," *Journal of Applied Mechanics*, Vol. 83, No. 11, 2016, p. 111005. https://doi.org/https://doi.org/10.1115/1.4034431.

[36] Derveni, F., Abbasi, A., and Reis, P. M., "Defect–Defect Interactions in the Buckling of Imperfect Spherical Shells," *Journal of Applied Mechanics*, Vol. 92, No. 4, 2025. https://doi.org/https://doi.org/10.1115/1.4062774.

[37] Groh, R., and Pirrera, A., "Probing the stability landscape of cylindrical shells for buckling knockdown factors," *Philosophical Transactions of the Royal Society A*, Vol. 381, No. 2244, 2023, p. 20220032. https://doi.org/https://doi.org/10.1098/rsta.2022.0032.

[38] Jiménez, F. L., Marthelot, J., Lee, A., Hutchinson, J. W., and Reis, P. M., "Technical brief: knockdown factor for the buckling of spherical shells containing large-amplitude geometric defects," *Journal of Applied Mechanics*, Vol. 84, No. 3, 2017, p. 034501. https://doi.org/https://doi.org/10.1115/1.4035665.

[39] Abbasi, A., Derveni, F., and Reis, P. M., "Comparing the buckling strength of spherical shells with dimpled versus bumpy defects," *Journal of Applied Mechanics*, Vol. 90, No. 6, 2023, p. 061008. https://doi.org/https://doi.org/10.1115/1.4056801.

[40] Yan, D., Pezzulla, M., and Reis, P. M., "Buckling of pressurized spherical shells containing a through-thickness defect," *Journal of the Mechanics and Physics of Solids*, Vol. 138, 2020, p. 103923. https://doi.org/https://doi.org/10.1016/j.jmps.2020.103923.

[41] Ubamanyu, U. K., Baizhikova, Z., Le, J.-L., Ballarini, R., and Reis, P. M., "A numerical study on the buckling of near-perfect spherical shells," *Journal of Applied Mechanics*, Vol. 92, No. 5, 2025, p. 051003. https://doi.org/https://doi.org/10.1115/1.4067852.

[42] Thompson, J. M. T., Hutchinson, J. W., and Sieber, J., "Probing shells against buckling: a nondestructive technique for laboratory testing," *International Journal of Bifurcation and Chaos*, Vol. 27, No. 14, 2017, p. 1730048. https://doi.org/https://doi.org/10.1142/S0218127417300488.

[43] Lee, A. J., and Fernandez, J. M., "Inducing bistability in Collapsible Tubular Mast booms with thin-ply composite shells," *Composite Structures*, Vol. 225, No. March, 2019, p. 111166. https://doi.org/https://doi.org/10.1016/j.compstruct.2019.111166.

[44] Leclerc, C., and Pellegrino, S., "Nonlinear elastic buckling of ultra-thin coilable booms," *International Journal of Solids and Structures*, Vol. 203, 2020, pp. 46–56. https://doi.org/https://doi.org/10.1016/j.ijsolstr.2020.06.042.

[45] Audoly, B., and Hutchinson, J. W., "Localization in spherical shell buckling," *Journal of the Mechanics and Physics of Solids*, Vol. 136, 2020, p. 103720. https://doi.org/https://doi.org/10.2514/8.10722.

[46] Hutchinson, J. W., and Thompson, J. M. T., "Nonlinear buckling behaviour of spherical shells: barriers and symmetry-breaking dimples," *Philosophical Transactions of the Royal Society A: Mathematical, Physical and Engineering Sciences*, Vol. 375, No. 2093, 2017, p. 20160154. https://doi.org/https://doi.org/10.1098/rsta.2016.0154.

[47] Royer, F., and Pellegrino, S., "Experimentally probing the stability of thin-shell structures under pure bending," *Philosophical Transactions of the Royal Society A: Mathematical, Physical and Engineering Sciences*, Vol. 381, No. 2244, 2023. https://doi.org/https://doi.org/10.1098/rsta.2022.0024.

[48] Groh, R., and Pirrera, A., "On the role of localizations in buckling of axially compressed cylinders," *Proceedings of the Royal Society A*, Vol. 475, No. 2224, 2019, p. 20190006. https://doi.org/https://doi.org/10.1098/rspa.2019.0006.